

A Note on Geodesics in Hayward Metric

Takeshi Chiba¹ and Masashi Kimura²

¹*Department of Physics, College of Humanities and Sciences,*

Nihon University, Tokyo 156-8550, Japan

² *CENTRA, Departamento de Fisica,*

Instituto Superior Tecnico-IST, Universidade de Lisboa-UL,

Avenida Rovisco Pais 1, 1049 Lisboa, Portugal

(Dated: December 3, 2024)

Abstract

We study timelike and null geodesics in a non-singular black hole metric proposed by Hayward. The metric contains an additional length-scale parameter ℓ and approaches the Schwarzschild metric at large radii while approaches a constant at small radii so that the singularity is resolved. We tabulate the various critical values of ℓ for timelike and null geodesics: the critical values for the existence of horizon, marginally stable circular orbit and photon sphere. We find the photon sphere exists even if the horizon is absent and two marginally stable circular orbits appear if the photon sphere is absent and a stable circular orbit for photons exists for certain range of ℓ . We visualize the image of a black hole and find that blight rings appear even if the photon sphere is absent.

PACS numbers: 98.80.Cq, 98.80.Es

I. INTRODUCTION

A non-singular model of a black hole was proposed by Hayward [1]. As such, it may be a solution of an ultraviolet complete gravity such as [2].

In this paper, we summarize the results of our study of the properties of geodesics in the geometry described by the Hayward metric in a self-contained manner. Some of the results may be already known (for example, [3, 4]), but the detailed study of both the properties of marginally stable circular orbits and the behaviour of null geodesics are new as far as we know.

In Sec. II, after giving the radii of the horizons of the spacetime, we study the properties of timelike geodesics and null geodesics. Sec. III is devoted to summary. In Appendix A, we summarize the properties of the geodesics in the the Reissner-Nordström metric.

We use the units of $G = c = 1$.

II. GEODESICS IN HAYWARD METRIC

The Hayward metric is given by [1]

$$ds^2 = -F(r)dt^2 + \frac{dr^2}{F(r)} + r^2 d\Omega^2 \quad (1)$$
$$F(r) = 1 - \frac{2Mr^2}{r^3 + 2\ell^2 M},$$

where M is a mass parameter and ℓ is a length-scale parameter. The metric approaches $1 - 2M/r$ as $r \rightarrow \infty$ and approaches unity smoothly as $r \rightarrow 0$ and hence is non-singular. The metric is “minimal” in the sense that it contains the least number of free parameters (ℓ only) with the desired properties (regularity at the center such that $F(r) \rightarrow 1 + \mathcal{O}(r^2)$ and Schwarzschild asymptotic behaviour at large radii. In fact, Frolov has recently shown that if $F(r)$ is a rational function of r , the order of the polynomials must be larger than of 2 and $F(r)$ constructed out of the polynomials of the order 3 contains two free parameters in general [5].

We may compute the effective energy momentum for the metric Eq. (2) via $T_{\mu\nu} = \frac{1}{8\pi}G_{\mu\nu}$ as done in [1].¹ Then, the energy density $\rho = -T^t_t$, the radial pressure $p_r = T^r_r$ and the

¹ The method for computing $T_{\mu\nu}$ in this way is sometimes called “Nariai method” in Japanese GR community.

tangential pressure $p_T = T^\theta_\theta = T^\phi_\phi$ are given by [1]

$$\rho = -p_r = \frac{12\ell^2 M^2}{(r^3 + 2\ell^2 M)^2}, \quad (2)$$

$$p_T = \frac{24\ell^2 M^2(r^3 - \ell^2 M)}{(r^3 + 2\ell^2 M)^3}, \quad (3)$$

and we find that the weak energy condition is satisfied: $\rho > 0, \rho + p_r = 0, \rho + p_T \geq 0$ and that the strong energy condition is violated for $r < (\ell^2 M)^{1/3}$ since $\rho + p_r + 2p_T = 2p_T$.

Henceforth, we normalize the length scale by M and introduce the following dimensionless parameter

$$a \equiv \frac{\ell}{M}, \quad (4)$$

and use $\tilde{r} = r/M$ as a dimensionless variable.

A. Horizon

The location of a horizon is determined by $F(r) = 0$, and horizons (outer horizon \tilde{r}_+ and inner horizon \tilde{r}_-) exist for $0 \leq a \leq a_H$ [1],

$$\tilde{r}_+ = \frac{2}{3} + \frac{4}{3} \cos \left(\frac{1}{3} \cos^{-1} \left(1 - \frac{27a^2}{8} \right) \right), \quad (5)$$

$$\tilde{r}_- = \frac{2}{3} - \frac{4}{3} \cos \left(\frac{1}{3} \cos^{-1} \left(1 - \frac{27a^2}{8} \right) + \frac{\pi}{3} \right), \quad (6)$$

where

$$a_H = \frac{4}{3\sqrt{3}} = 0.7698\dots \quad (7)$$

The upper bound on a implies the lower bound on M , $M \geq a_H \ell$. The implications of this lower bound on the formation and the evaporation of black holes are discussed in [1]. In Fig. 1, we show the radii of the horizons (black curve). The causal structure is quite similar to the Reissner-Nordström black hole: $a < a_H, a = a_H, a > a_H$ corresponds to $Q < M, Q = M, Q > M$ Reissner-Nordström black hole, only exception being that the central singularity is replaced with a regular center.

B. Timelike Geodesics

From the spherical symmetry, we may restrict ourselves to the equatorial plane without loss of generality. In terms of two conserved quantities, the energy $E = F(r)\dot{t}$ and the

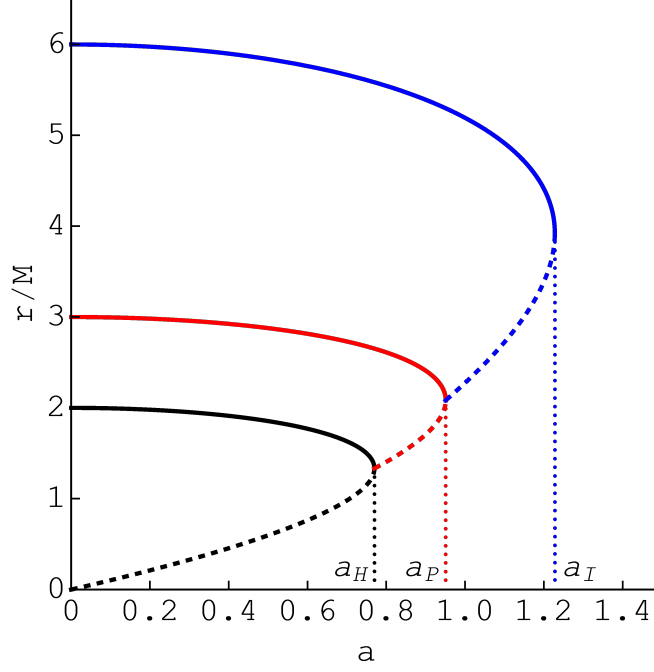


Figure 1: The radii of horizons (black) (outer: solid; inner: dashed), ISCO or marginally stable circular orbit (blue), photon sphere (red solid) and stable circular orbit of photon (red dashed). Dotted vertical lines are critical values of $a = \ell/M$ (a_H, a_P, a_I from left).

angular momentum $L = r^2 \dot{\phi}$, the timelike geodesics satisfy the following energy equation

$$\frac{1}{2} \dot{r}^2 + V(r) = \frac{1}{2} E^2, \quad V(r) = \frac{1}{2} \left(1 + \frac{L^2}{r^2} \right) F(r), \quad (8)$$

where $\dot{t} = dt/d\tau$ with τ being the proper time.

A marginally stable circular orbit (MSCO) is determined by the condition $V' = V'' = 0$ which reduces to the following equation for r ²

$$\tilde{r}^6 - 6\tilde{r}^5 + 22a^2\tilde{r}^3 - 32a^4 = 0, \quad (9)$$

and the innermost of such an orbit is called the innermost stable circular orbit (ISCO). L^2 is determined by

$$\left(\frac{L}{M} \right)^2 = \frac{\tilde{r}^3 dF/d\tilde{r}}{2F - \tilde{r} dF/d\tilde{r}} = \frac{\tilde{r}^7 - 4a^2\tilde{r}^4}{4a^4 + 4a^2\tilde{r}^3 + (\tilde{r} - 3)\tilde{r}^5}. \quad (10)$$

² If $F(r) = 1 - Q_{n-1}(r)/P_n(r)$, where $P_n(r)$ and $Q_{n-1}(r)$ are polynomials of order n and $n-1$, respectively, the degree of the equation becomes $3n-3$.

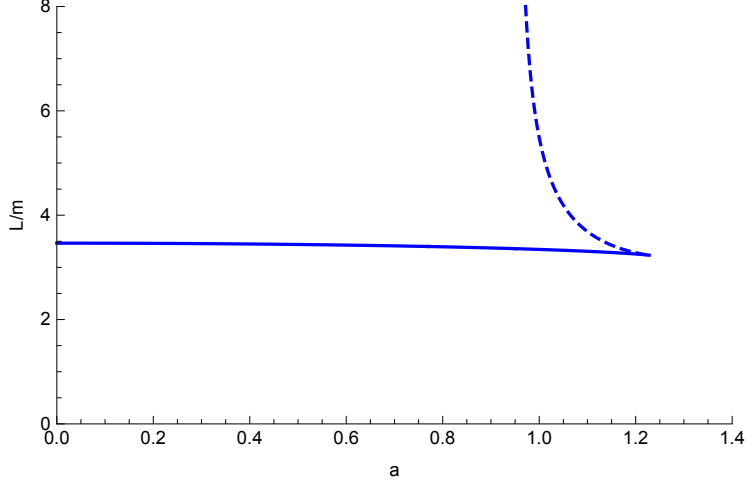


Figure 2: The angular momentum of marginally stable circular orbits. Solid (dashed) curve corresponds to blue solid (dashed) curve in Fig. 1.

We find that Eq. (9) has one positive real solution for $a < a_H$ and three positive real solutions for $a_H < a < a_I$ and one positive real solution for $a > a_I$, where a_I is given by

$$a_I = \frac{200}{51} \sqrt{\frac{5}{51}} = 1.2278\dots \quad (11)$$

However, both two of the solutions for $a_H < a < a_P$ and one solution for $a > a_P$ are turned out to have imaginary L and are unphysical, where

$$a_P = \frac{25}{24} \sqrt{\frac{5}{6}} = 0.9509\dots, \quad (12)$$

so there is no ISCO for $a > a_I$. After all, there is one ISCO for $a < a_P$ and two MSCOs for $a_P < a < a_I$ and no ISCO for $a > a_I$. In Fig. 1 and Fig.2, we show the radii of ISCO or MSCO (blue curve) and the angular momentum. The angular momentum of the inner MSCO for $a_H < a < a_I$ is arbitrary large as $a \rightarrow a_P$.

In Fig. 3, we show the allowed region for the stable circular orbit (gray). Light gray region in the middle is the unstable orbit $d^2V/dr^2 < 0$. Lower white region is forbidden because the angular momentum is imaginary or the radius is inside the horizon.

In order to study the properties of circular orbits, we calculate the energy of a particle in circular orbit as a function the radius for $a = 0.5, 0.9, 1$ as shown in Fig. 4. The extrema of the energy correspond to MSCOs: for $a = 1$ the minimum is the outer MSCO and the maximum is the inner MSCO. The region in between two MSCOs (dashed curve) is unstable because $d^2V/dr^2 < 0$ there. The outer MSCO can be reached from a particle in circular orbit

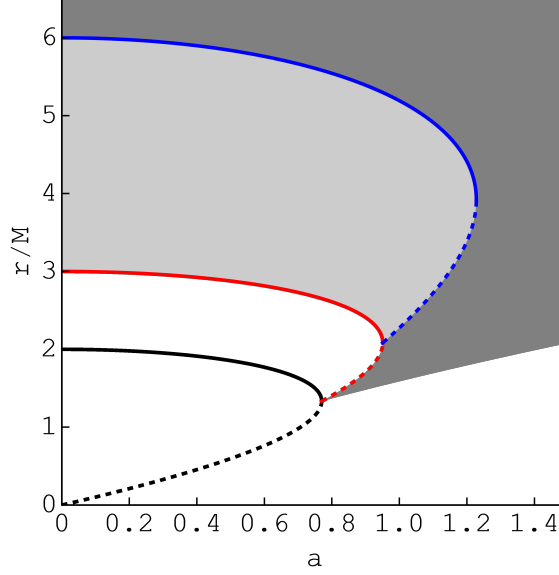


Figure 3: The region of stable circular orbit (gray) as a function of a . Light gray region in the middle is the unstable orbit. Lower white region is forbidden because either the angular momentum is imaginary or the radius is inside the horizon. Blue (ISCO), red (photon sphere and circular null geodesics) and black (horizons) curves are the same as Fig. 1.

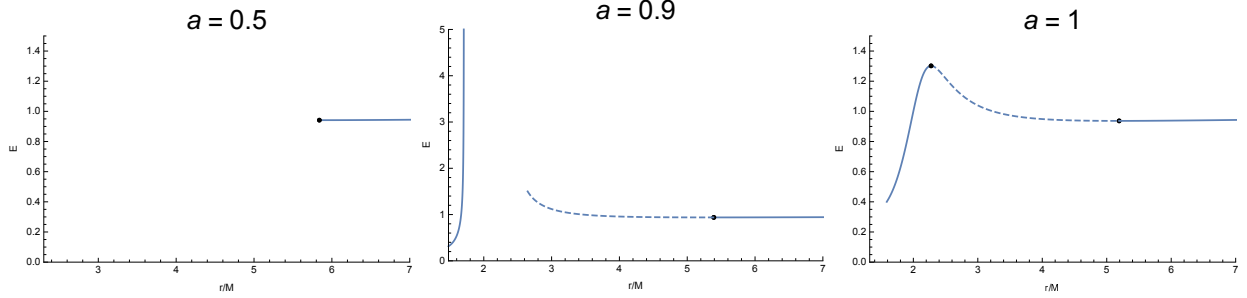


Figure 4: The energy of a particle in circular orbit as a function of the radius of the orbit for $a = 0.5, 0.9, 1$ from left to right. Black dots correspond to marginally stable circular orbits. The circular orbit is unstable for dashed curve.

outside by its emitting energy and angular momentum. On the other hand, since the energy of the inner MSCO is larger than 1 (the energy at large r), the inner MSCO is unbound and may be regarded as an “excited state” cannot reached from a particle in circular orbit outside. In this sense, only the outer MSCO may be physically important. For $a = 0.9$, there is also a stable circular orbit with large L and $E > 1$.

C. Null Geodesics

As in the case of the timelike geodesics, in terms of E and L , the null geodesics satisfy

$$\frac{1}{2}\dot{r}^2 + V_{\text{null}}(r) = \frac{1}{2}E^2, \quad V_{\text{null}}(r) = \frac{L^2}{2r^2}F(r), \quad (13)$$

where $\dot{r} = dr/d\lambda$ with λ being the affine parameter.

Since L/E is the impact parameter at large r , the (local) maximum of the effective potential $V_{\text{null}}(r)$ determines the capture cross section for photons and hence the size of shadow of a black hole: photons with smaller impact parameter will be captured by the black hole. The location of the (local) maximum of $V_{\text{null}}(r)$, or the radius of unstable circular orbits of photons (photon sphere [6]), r_P , is determined by

$$\tilde{r}^6 - 3\tilde{r}^5 + 4a^2\tilde{r}^3 + 4a^4 = 0. \quad (14)$$

Similar to the case of ISCO, we find that the maximum of $V_{\text{null}}(r)$ exists if $a < a_P$, where a_P is defined in Eq. (12). In Fig. 1 we show the radius of photon sphere (red solid). There also appears a stable circular orbit of photon (red dashed) for $a < a_P$. The appearance of a stable circular photon orbit is inevitable in the presence of the photon sphere (local maximum of V_{null}) since V_{null} positively diverges as $r \rightarrow 0$.³ In Fig. 5, we show the radius of the shadow b_P defined by

$$b_P = \sqrt{\frac{L^2}{2V_{\text{null}}(r_P)}} = \frac{r_P}{\sqrt{F(r_P)}} \quad (15)$$

In order to study the effect of the geometry on the propagation of light rays, we first compute the deflection of light in the Hayward metric. We consider the deflection of light in the equatorial plane. Then from Eq. (13) and $L = r^2\dot{\phi}$, in terms of the impact parameter $b = L/E$, up to the turning point of the deflection, ϕ satisfies

$$r^2 \frac{d\phi}{dr} = \left(b^{-2} - \frac{F(r)}{r^2} \right)^{-1/2}. \quad (16)$$

Denoting the turning point of the deflection as r_0 at which $V_{\text{null}}(r_0) = E^2/2$ or $b^{-2} = F(r_0)/r_0^2$, the deflection angle $\Delta\phi$ is then given by

$$\Delta\phi = 2 \int_0^{1/r_0} \frac{du}{\sqrt{b^{-2} - u^2 F(1/u)}} - \pi, \quad (17)$$

³ The presence of a stable photon orbit, however, would be problematic because perturbations can become long-lived and nonlinear effects may destabilize the system [7].

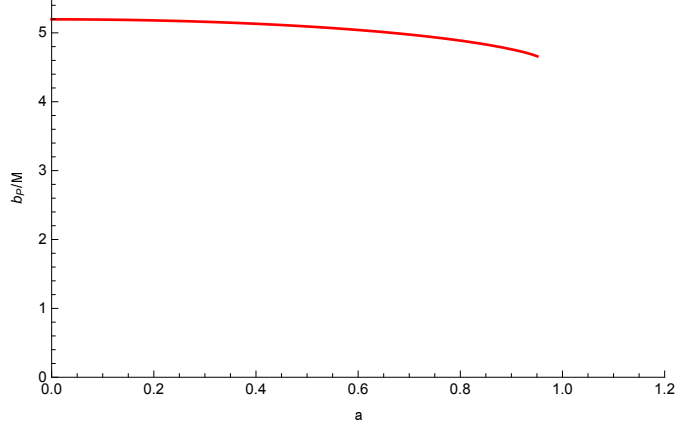


Figure 5: Shadow radius b_P as a function of $a = \ell/M$.

where we have made the change of variables by $u = 1/r$ as usual. Expanding in terms of M/r_0 under the assumption $\Delta\phi$ is small (weak deflection), the result is

$$\begin{aligned} \Delta\phi = & \frac{4M}{r_0} + \frac{(15\pi - 16)}{4} \left(\frac{M}{r_0}\right)^2 + \frac{(244 - 45\pi)}{6} \left(\frac{M}{r_0}\right)^3 + \left(-130 + \frac{3465\pi}{64} - \frac{15\pi}{4}a^2\right) \left(\frac{M}{r_0}\right)^4 \\ & + \left(\frac{7783}{10} - \frac{3465\pi}{16} + \frac{75\pi - 472}{5}a^2\right) \left(\frac{M}{r_0}\right)^5 \\ & + \left(\frac{310695\pi}{256} - \frac{21397}{6} + \frac{5}{16}(1664 - 693\pi)a^2\right) \left(\frac{M}{r_0}\right)^6 + O\left(\left(\frac{M}{r_0}\right)^7\right). \end{aligned} \quad (18)$$

We only show the result up to $O((M/r_0)^6)$, although we can calculate arbitrary higher orders. The coefficients for $a = 0$ fully agree with [8], but the sign of the coefficient of $(M/r_0)^4$ including a is different from [3] in which only the numerical values of the coefficient are given and higher order terms are not given. In terms of the impact parameter b using $b^{-2} = F(r_0)/r_0^2$, the deflection angle up to $O((M/b)^6)$ is given by

$$\begin{aligned} \Delta\phi = & \frac{4M}{b} + \frac{15\pi}{4} \left(\frac{M}{b}\right)^2 + \frac{128}{3} \left(\frac{M}{b}\right)^3 + \left(\frac{3465\pi}{64} - \frac{15\pi}{4}a^2\right) \left(\frac{M}{b}\right)^4 \\ & + \left(\frac{3584}{5} - \frac{512a^2}{5}\right) \left(\frac{M}{b}\right)^5 + \left(\frac{255255\pi}{256} - \frac{3465\pi}{16}a^2\right) \left(\frac{M}{b}\right)^6 + O\left(\left(\frac{M}{b}\right)^7\right) \end{aligned} \quad (19)$$

Again, we find that a complete agreement with [8] up to this order if $a = 0$. Since the effect of nonzero a only appears from $O((M/b)^4)$ and beyond, it is difficult to detect the effect by the (weak) deflection angle. From the requirement that the fourth term should not dominate the first term by 0.001% [9], a is only constrained as $a \lesssim 10^5(b/R_\odot)^{3/2}(M/M_\odot)^{-3/2}$ or $\ell \lesssim 10^5 \text{km}(b/R_\odot)^{3/2}(M/M_\odot)^{-1/2}$.

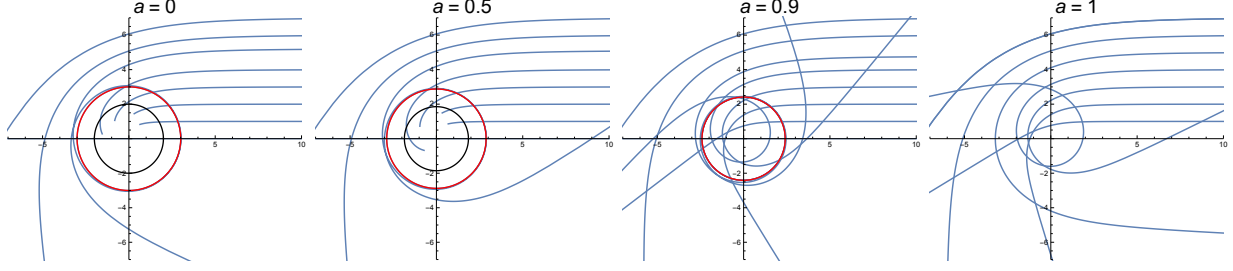


Figure 6: Trajectories of light rays (coming in from upper right) for $a = 0, 0.5, 0.9, 1$ from left to right. A black circle is the (outer) horizon, red circles are the radii of photon spheres.

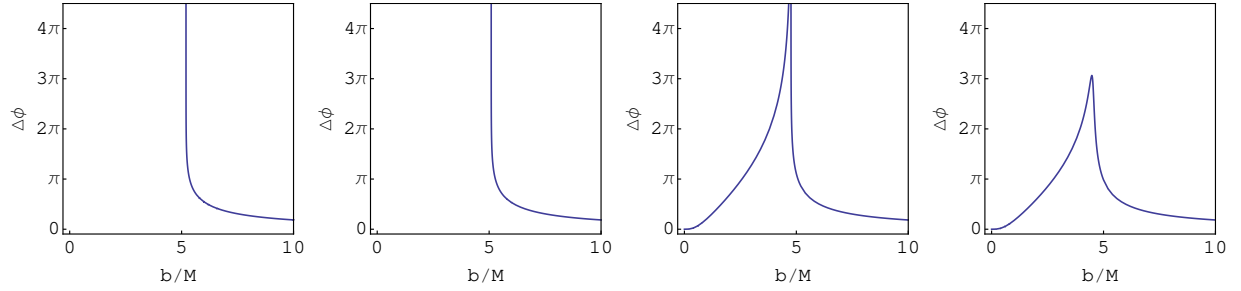


Figure 7: The deflection angle as a function of the impact parameter b for $a = 0, 0.5, 0.9, 1$ from left to right.

However, the presence of a does affect the existence or nonexistence of the photon sphere and hence affect the behaviour of light rays traveling around the photon sphere. In Fig. 6, we show the trajectories of light rays coming in from upper right for $a = 0, 0.5, 0.9, 1$. A black circle is the (outer) horizon, red circles are the radii of photon spheres. In Fig. 7, we

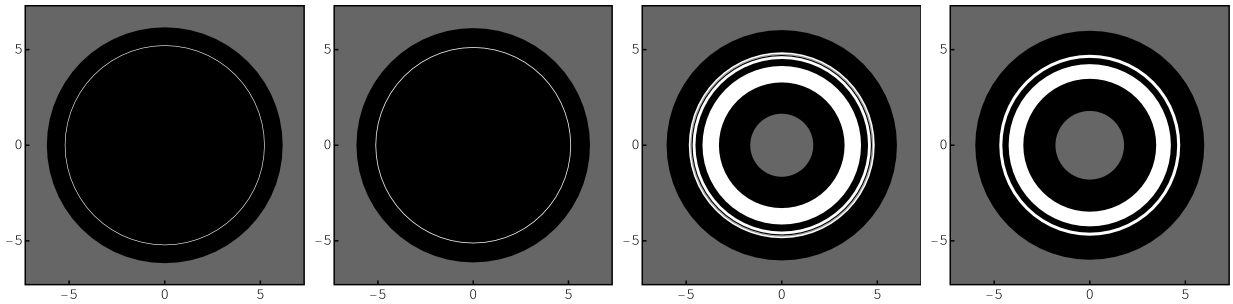


Figure 8: Image of a non-singular black hole described by Hayward metric for $a = 0, 0.5, 0.9, 1$ from left to right. Photons in the black region never reach the observer. Photons in the white region travel around the central region more than once, while photons in gray regions reach the observer straightforwardly.

show the deflection angle as a function of the impact parameter b for $a = 0, 0.5, 0.9, 1$. If the impact parameter is slightly larger than the radius of a shadow b_P , the deflection angle $\Delta\phi$ is logarithmically divergent as

$$\Delta\phi \sim \frac{1}{\sqrt{-5 + 2\sqrt{3r_P/M}}} \ln(b - b_P)^{-1}, \quad (20)$$

If $a = a_P$, *i.e.*, $r_P = 25/12$, the divergent behavior is changed into

$$\Delta\phi \sim c_0 M^{1/6} (b - b_P)^{-1/6}, \quad (21)$$

$$c_0 = 2^{11/6} 3^{2/3} 5^{5/4} \int_0^\infty dy \frac{1}{\sqrt{432y + 900y^2 + 625y^3}} \simeq 7.771. \quad (22)$$

A quite similar behaviour is also found for the Reissner-Nordström metric where critical values corresponding to a_H, a_P appear depending on the value of the charge (Appendix A).

The images of a “black hole” are shown in Fig 8. Photons in black regions never reach the observer due to the presence of a horizon or the deflection angle being $\pm\pi/2$ (modulo 2π). Photons in white regions travel around the central region more than once, while photons in gray regions reach the observer straightforwardly. The image for $a = 0.5$ is little different from that of Schwarzschild black hole ($a = 0$): A blight ring surrounding a black disk (shadow of a black hole) appears. Interestingly, for $a = 0.9$ ($a_H < a < a_P$), the photon sphere exists even though the horizon is absent, and a black disk disappears and a black doughnut appears instead and a ring image persists. More interestingly, even for $a = 1$ ($> a_P$), the ring persists although the photon sphere is absent as shown in Fig. 8. Therefore, the existence of a blight ring image does not necessarily imply the existence of a photon sphere. Of course, for astrophysical black holes $a \simeq 10^{-38}(\ell/\ell_P)(M_\odot/M) \ll 1$, where ℓ_P is the Planck length, and these phenomena would be expected only for Planck-scale primordial black holes.

III. SUMMARY

In this paper, we have studied the timelike and null geodesics in a non-singular black hole geometry proposed by Hayward which involves a parameter ℓ and found several interesting features of the geometry: the existence or non-existence of the horizon, the photon sphere and the ISCO. We also have found that two marginally stable circular orbits appear for $a_H < \ell/M < a_P$ although the inner orbit is unbound. The existence of a horizon and/or a photon sphere significantly affect the behaviour of the null geodesics. We have found that

a black doughnut appears if the horizon is absent and that blight rings appear even if the photon sphere is absent.

One may think that bright regions in a shadow image are due to the existence of the photon sphere. However, as shown in Fig.8, bright regions also can appear in the spacetime with no photon sphere if the parameter a is slightly larger than a_P . In such parameters, while there are no photon sphere, $\Delta\phi$ can still take a value larger than 2π (see Fig.7). The similar behavior can be found in the Reissner-Nordström metric. These results suggest that such the shadow images are universal behavior for parameters slightly larger than the critical value where photon sphere marginally exists. The parameter ℓ is currently only loosely constrained by the solar-system experiment since the deflection angle at the post-Newtonian order is the same as that of Schwarzschild. If the shadow of a black hole is observed, we may put an $O(1)$ constraint on ℓ/M .

ACKNOWLEDGEMENTS

This work is supported by the Grant-in-Aid for Scientific Research from JSPS (Nos.24540287) and in part by Nihon University. M.K. acknowledges financial support provided under the European Union’s H2020 ERC Consolidator Grant “Matter and strong-field gravity: New frontiers in Einstein’s theory” grant agreement no. MaGRaTh-646597, and under the H2020-MSCA-RISE-2015 Grant No. StronGrHEP-690904.

Appendix A: Reissner-Nordström metric

The Reissner-Nordström metric is given by

$$ds^2 = -F(r)dt^2 + \frac{dr^2}{F(r)} + r^2 d\Omega^2 \quad (\text{A1})$$

$$F(r) = 1 - \frac{2M}{r} + \frac{Q^2}{r^2},$$

where M, Q are mass and electric charge parameters, respectively. We study the property of geodesics on this metric and compare the result with the case of the Hayward metric.

Since the electric charge parameter appears in the metric as Q^2 , we only need to consider $Q \geq 0$. If $1 \geq Q/M$, there are two horizons at $r = r_{\pm} = M^2 \pm \sqrt{M^2 - Q^2}$. In Fig.9, we plotted the region of stable and unstable circular orbits. The qualitative feature is same as

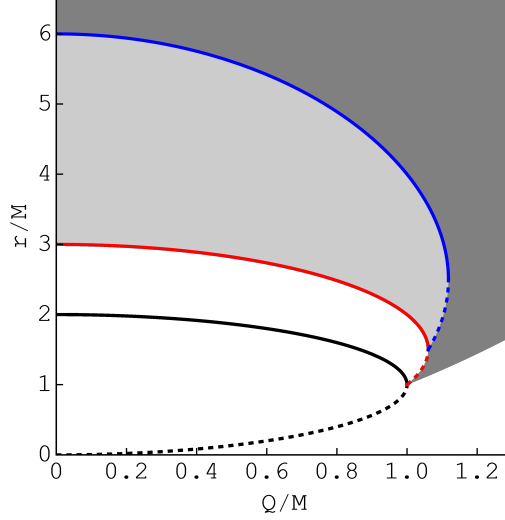


Figure 9: The region of stable and unstable circular orbits as a function of Q/M .

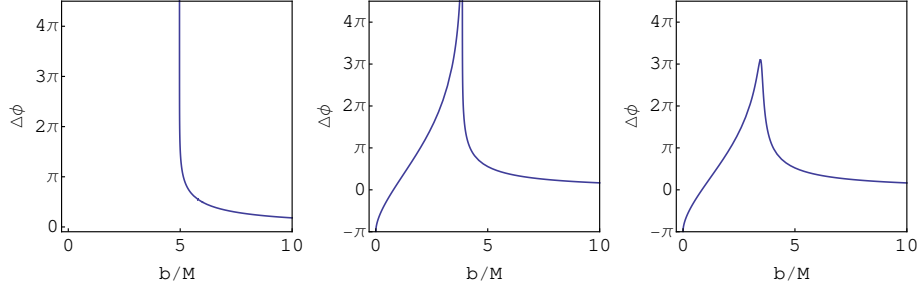


Figure 10: The deflection angle as a function of the impact parameter b for $Q/M = 0.5, 1.03, 1.08$ from left to right.

the case of the Hayward metric Fig.3. When Q/M takes $Q_H/M = 1, Q_P/M = 3/(2\sqrt{2}) \simeq 1.061, Q_I/M = \sqrt{5}/2 \simeq 1.118$, the horizon becomes extremal, the photon sphere marginally exists, the ISCO marginally exists, respectively. The location of the photon sphere and the shadow image for The Reissner-Nordström metric is also discussed in [10].

Fig.10 shows the deflection angle for null geodesics as a function of the impact parameter b . Compared to the case of the Hayward metric (see Fig.7), the qualitative behavior is almost the same. The only difference can be found near the region for small impact parameter $b \simeq 0$ in overcharged cases $Q/M > 1$, where the deflection angle $\Delta\phi$ takes almost $-\pi$. This is because the null geodesic is reflected by the repulsive force near the origin $r = 0$.

If we consider $Q > Q_P$, there is no photon sphere. However, for the parameter slightly larger than Q_P (see the third figure in Fig.10), $\Delta\phi$ can still take the value larger than 2π .

This means that their shadow image is similar to the fourth figure in Fig.8.

-
- [1] S. A. Hayward, Phys. Rev. Lett. **96**, 031103 (2006) doi:10.1103/PhysRevLett.96.031103 [gr-qc/0506126].
 - [2] T. Biswas, E. Gerwick, T. Koivisto and A. Mazumdar, Phys. Rev. Lett. **108**, 031101 (2012) doi:10.1103/PhysRevLett.108.031101 [arXiv:1110.5249 [gr-qc]].
 - [3] S. W. Wei, Y. X. Liu and C. E. Fu, Adv. High Energy Phys. **2015**, 454217 (2015) doi:10.1155/2015/454217 [arXiv:1510.02560 [gr-qc]].
 - [4] J. Schee and Z. Stuchlik, JCAP **1506**, 048 (2015) doi:10.1088/1475-7516/2015/06/048 [arXiv:1501.00835 [astro-ph.HE]].
 - [5] V. P. Frolov, Phys. Rev. D **94**, no. 10, 104056 (2016) doi:10.1103/PhysRevD.94.104056 [arXiv:1609.01758 [gr-qc]].
 - [6] K. S. Virbhadra and G. F. R. Ellis, Phys. Rev. D **62**, 084003 (2000) doi:10.1103/PhysRevD.62.084003 [astro-ph/9904193].
 - [7] V. Cardoso, L. C. B. Crispino, C. F. B. Macedo, H. Okawa and P. Pani, Phys. Rev. D **90**, no. 4, 044069 (2014) doi:10.1103/PhysRevD.90.044069 [arXiv:1406.5510 [gr-qc]].
 - [8] C. R. Keeton and A. O. Petters, Phys. Rev. D **72**, 104006 (2005) doi:10.1103/PhysRevD.72.104006 [gr-qc/0511019].
 - [9] B. Bertotti, L. Iess and P. Tortora, Nature **425**, 374 (2003).
 - [10] A. F. Zakharov, Phys. Rev. D **90**, no. 6, 062007 (2014) doi:10.1103/PhysRevD.90.062007 [arXiv:1407.7457 [gr-qc]].